Unfolding Genus-2 Orthogonal Polyhedra with Linear Refinement

Noname manuscript No.
(will be inserted by the editor)

Unfolding Genus-2 Orthogonal Polyhedra with Linear Refinement

Mirela Damian · Erik Demaine · Robin Flatland · Joseph O'Rourke

the date of receipt and acceptance should be inserted later

Abstract We show that every orthogonal polyhedron of genus $g \leq 2$ can be unfolded without overlap while using only a linear number of orthogonal cuts (parallel to the polyhedron edges). This is the first result on unfolding general orthogonal polyhedra beyond genus-0. Our unfolding algorithm relies on the existence of at most 2 special leaves in what we call the "unfolding tree" (which ties back to the genus), so unfolding polyhedra of genus 3 and beyond requires new techniques.

Keywords grid unfolding, linear refinement, orthogonal polyhedron, genus 2

1 Introduction

An *unfolding* of a polyhedron is produced by cutting its surface in such a way that it can be flattened to a single, connected piece without overlap. In an *edge unfolding*, the cuts are restricted to the polyhedron's edges, whereas in a *general unfold-*

M. Damian
Department of Computer Science
Villanova University
Villanova, PA 19085, USA
E-mail: mirela.damian@villanova.edu

E. Demaine
Computer Science and Artificial Intelligence Laboratory
Massachusetts Institute of Technology
32 Vassar St., Cambridge, MA 02139, USA
E-mail: edemaine@mit.edu

R. Flatland
Department of Computer Science
Siena College
Loudonville, NY 12211, USA
E-mail: flatland@siena.edu

J. O'Rourke
Department of Computer Science
Smith College
Northampton, MA 01063, USA
E-mail: jorourke@smith.edu

ing, cuts can be made anywhere on the surface. It is known that edge cuts alone are not sufficient to guarantee an unfolding for non-convex polyhedra [BDE$^+$03, BDD$^+$98], and yet it is an open question as to whether all non-convex polyhedra have a general unfolding. In contrast, it is unknown whether every convex polyhedron has an edge unfolding [DO07, Ch. 22], but all convex polyhedra have general unfoldings [DO07, Sec. 24.1.1].

The successes to date in unfolding non-convex objects have been with the class of orthogonal polyhedra. This class consists of polyhedra whose edges and faces all meet at right angles. Because not all orthogonal polyhedra have edge unfoldings (even for simple examples such as a box with a smaller box extruding out on top) [BDD$^+$98], the unfolding algorithms use additional non-edge cuts. These additional cuts generally follow one of two models. In the *grid unfolding model*, the orthogonal polyhedron is sliced by axis perpendicular planes passing through each vertex, and cuts are allowed along the slicing lines where the planes intersect the surface. In the *grid refinement model*, each rectangular grid face under the grid unfolding model is further subdivided by an $(a \times b)$ orthogonal grid, for some positive integers $a, b \geq 1$, and cuts are also allowed along any of these grid lines.

There have been three phases of research on unfolding orthogonal polyhedra. The first phase focused on unfolding special subclasses, which included orthotubes [BDD$^+$98], well-separated orthotrees [DFMO05], orthostacks [BDD$^+$98, DM04], and Manhatten towers [DFO08]. These algorithms use the grid unfolding model or the grid refinement model with a constant amount of refinement (i.e., a and b are both constants).

The second phase began with the discovery of the epsilon-unfolding algorithm [DFO07] which unfolds all genus-0 orthogonal polyhedra. A key component of the unfolding algorithm is the determination of a spiral path on the surface of the polyhedron that unfolds to a planar monotone staircase, from which the rest of the surface attaches (without overlap) above and below. A drawback of that algorithm is that it requires an exponential amount of grid refinement. Subsequent improvements, however, reduced the amount of refinement to quadratic [DDF14], and then to linear [CY15], with both algorithms following the basic outline of [DFO07].

The third phase of research addresses the next obvious challenge, that of unfolding higher genus polyhedra. To our knowledge, the only attempt at this is that of Liou et al. [LPW14]. They provide an algorithm for unfolding a special subclass of one-layer orthogonal polyhedra in which all faces are unit squares and the holes are unit cubes.

Thus the question of whether all orthogonal polyhedra of genus greater than zero can be unfolded is still wide open, and is in a sense the natural endpoint of this line of investigation. In this paper we take a significant step toward this goal by presenting a new algorithm that unfolds all orthogonal polyhedra of genus 1 or 2. The algorithm extends ideas from [CY15] by making several key modifications to circumvent issues that arise from the presence of holes. As in [CY15], our algorithm only requires linear refinement.

1.1 Notation and Definitions

Let P be an orthogonal polyhedron of genus $g \leq 2$, whose edges are parallel to the coordinate axes and whose surface is a 2-manifold. We take the z-axis to define the *vertical* direction, the x-axis to determine *left* and *right*, and the y-axis to determine *front* and *back*. We consistently take the viewpoint from $y = -\infty$. The faces of P are distinguished by their outward normal: forward is $-y$; rearward is $+y$; left is $-x$; right is $+x$; bottom is $-z$; and top is $+z$.[1]

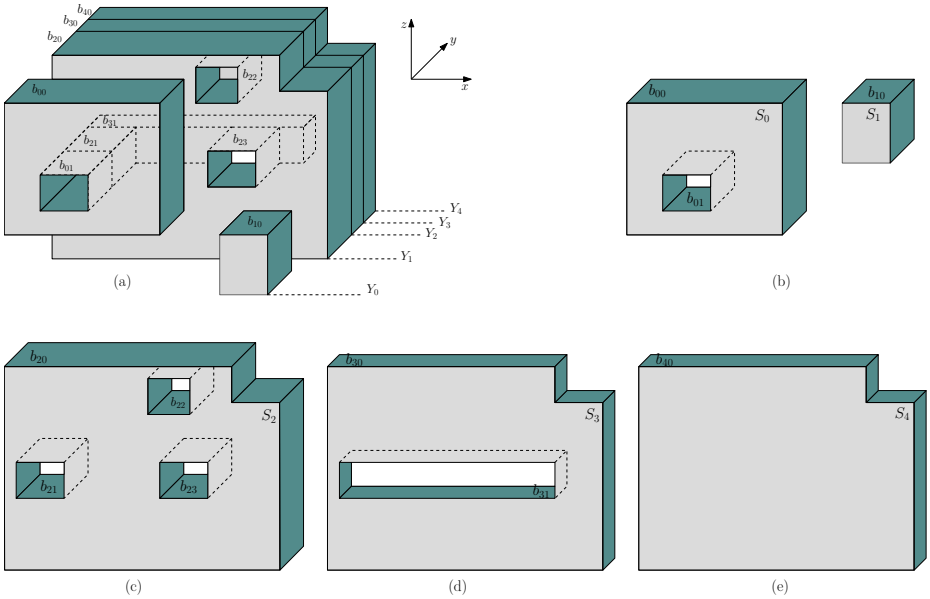

Fig. 1 (a) A polyhedron of genus one (bands are dark-shaded) (b) slabs S_0 (with bands b_{00} and b_{01}) and S_1 (with band b_{10}) delimited by Y_0 and Y_1; (c) slab S_2 (with bands b_{20}, b_{21}, b_{22} and b_{23}) delimited by Y_1 and Y_2; (d) slab S_3 (with bands b_{30} and b_{31}) delimited by Y_2 and Y_3, and (e) slab S_4 (with band b_{40}) delimited by Y_3 and Y_4.

Imagine slicing P with y-perpendicular planes through each vertex. Let Y_0, Y_1, Y_2, ... be the slicing planes sorted by y coordinate. Each (solid) connected component of P located between two consecutive planes Y_i and Y_{i+1} is called a *slab*. For example, the polyhedron from Figure 1a has five slabs S_0, S_1, S_2, S_3 and S_4, which are depicted in Figure 1(b-e). Note that each slab is an extruded orthogonal polygon with zero or more orthogonal holes, extruded in the y-direction. The cycle of {left, right, top, bottom} faces surrounding either the entire slab or a hole in a slab is called a *band*. Each slab has exactly one *outer* band, and zero or more *inner* bands. Referring to the example from Figure 1, the slab S_0 has outer band b_{00} and inner band b_{01}; S_1 has outer band b_{10} and no inner bands; S_2 has outer band b_{20} and inner bands b_{21}, b_{22} and b_{23}; S_3 has outer band b_{30} and inner band b_{31}; and S_4 has outer band b_{40} and no inner bands. Note that each band is associated with

[1] The $\pm y$ faces are given the awkward names "forward" and "rearward" to avoid confusion with other uses of "front" and "back" introduced later.

a unique slab. The intersection of a band with an adjacent plane Y_i (and similarly in Y_{i+1}) is a cycle of edges called a *rim* (so each band has exactly two rims).

We say that a rim r *encloses* a face of P if the portion of the Y-plane interior to r is a face of P. In other words, all points enclosed by r in the Y-plane are also on the surface of P. If there are points of the Y-plane enclosed by r that are not on the surface of P, then we say that r does not enclose a face of P. For example, in Figure 1 the rim of b_{10} in plane Y_0, the rim of b_{22} in plane Y_2 and the rim of b_{40} in plane Y_4 each enclose a face of P, but the rim of b_{00} in Y_0 does not.

2 Overview of Linear Unfolding

Throughout this section, P is an orthogonal polyhedron of genus zero. We begin with an overview of the algorithm in [CY15] that unfolds P using linear refinement. In Section 3 we will detail those aspects of the algorithm that we modify to handle orthogonal polyhedra of genus 1 and 2.

2.1 Unfolding Extrusions

Nearly all algorithmic issues in the linear unfolding algorithm from [CY15] are present in unfolding polyhedra that are vertical extrusions of simple orthogonal polygons. Therefore, we describe their unfolding algorithm for this simple shape class first, before extending the ideas to all orthogonal polyhedra of genus zero.

Before going into details, we briefly describe the algorithm at a high level. It begins by slicing P into slabs using y-perpendicular planes. For these vertical extrusions, all the slabs are boxes. The adjacency graph of these boxes is a tree T. Each leaf node b in T has a corresponding thin spiral surface path that includes a vertical segment running across the back face of b (which must be a face of P) on the side opposite to b's parent. The surface path extends from the bottom endpoint of this vertical segment by cycling around b's band until it reaches the top endpoint, and from there it continues along two strands that spiral side-by-side together on P, cycling around the bands on the path in T to the root node box where the two strands terminate. At the root box, the endpoints of all the pairs of strands are carefully stitched together into one surface path that can be flattened in the plane as a monotone staircase. By thickening the surface path to cover the band faces of P, and attaching the y-perpendicular faces above and below it, the entire surface of P is flattened without overlap into the plane. Details of the algorithm are provided in the sections that follow.

2.1.1 Unfolding Tree T

Again we restrict our attention to the situation where P is a vertical extrusion of a simple orthogonal polygon, and describe the algorithm in detail. The unfolding algorithm begins by slicing P with Y_i planes passing through every vertex, as described in Section 1. This induces a partition of P into rectangular boxes. See Figure 2a for an example. The dual graph of this partition is a tree T whose nodes correspond to bands, and whose edges connect pairs of adjacent bands. Figure 2b shows the tree T for the example from Figure 2a. We refer to T as the

unfolding tree, since it will guide the unfolding process. For simplicity, we will use the terms "node" and "band" interchangeably.

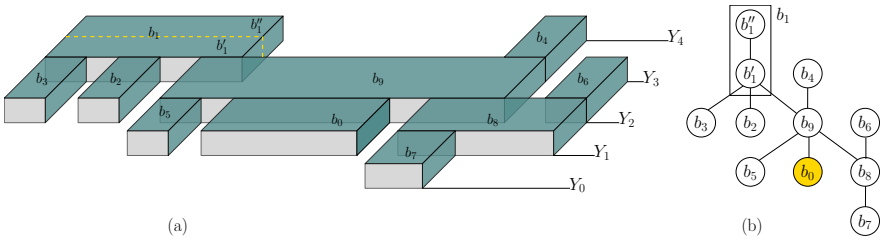

Fig. 2 (a) Genus-0 polyhedron partitioned into boxes (b) Unfolding tree T rooted at b_0.

Every tree of two or more nodes has at least two nodes of degree one, so we designate the root of T to be one of these degree-1 nodes. In Figure 2b for example, we may choose b_0 as the root of T, although any of the other degree-1 nodes would serve as well. The rim of the root band that has no adjacent band is called its *front* rim; the other rim is its *back* rim. For any other band b, the rim adjacent to b's parent in T is the *front* rim of b, and the other rim of b is its *back* rim. Children attached to the front rim of their parent are *front children*; children attached along the back rim of their parent are *back children*. Note that "front" and "back" modifiers for rims and children derive from the structure of T, and are not related to the "forward" and "rearward" $\pm y$ directions.

For reasons that will become clear later, we slightly alter the structure of T to eliminate all non-leaf nodes without back children. For each such internal band b, we perform a cut around its middle with a y-perpendicular plane. This partitions b into two bands b' and b'', with b' at the front and b'' at the back of b. This change in the partition is mirrored in T by replacing b with b', and adding b'' as a back leaf child of b'. In Figure 2, node b_1 is replaced by b_1' and b_1''. Thus each non-leaf node in T has at least one back child.

2.1.2 Leaf Node Unfolding

The unfolding of a leaf node b is determined by a spiral surface path whose endpoints lie on a top rim segment shared by b and its parent (necessarily on b's front rim, by definition). See Figure 3a where the endpoints are labeled e_1 and e_2. Observe that the middle of the path consists of a vertical segment on b's back face, shown in red on the exploded view of the back face in Figure 3a and circled in Figure 3b. We describe the spiral path as it extends out from the top and bottom of this segment to connect up with the endpoints on the front rim. From the bottom of the segment, the path moves parallel to the y-axis on the bottom face and then cycles counterclockwise to the top face where it meets up with the top end of the vertical segment. From there, both ends of the path cycle side-by-side together in a counterclockwise direction while displacing toward the front rim. We refer to this spiral path as the *connector path*, suggestive of its ability to connect two points (e_1 and e_2) that are both located on the same rim. When unfolded and laid horizontally in the plane, this spiral forms a monotone staircase, as depicted in Figure 3b.

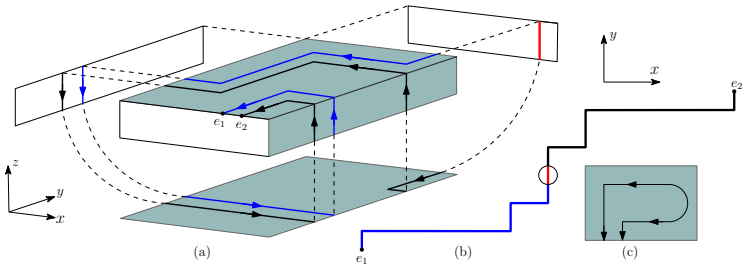

Fig. 3 Unfolding a leaf band in counterclockwise direction; arrows indicate the direction followed by the unfolding algorithm, starting at the back face vertical segment (shown in red in (a) and circled in (b) of this figure).

Three-dimensional illustrations, such as the one in Figure 3a, become impractical for more complex examples, so we will use instead the 2D representation depicted in Figure 3c. This 2D representation captures the counterclockwise direction of the blue and black portions of the path in Figure 3a, viewed from $y = -\infty$ as they cycle side-by-side together from the back to the front rim; the arc symbolizes the vertical back face segment connecting them.

A crucial property required by the Chang and Yen's unfolding algorithm [CY15] and the algorithms from which that derives [DFO07, DDF14] is that the back rim of each leaf band in T encloses a face of P. This is necessary because the connector paths use a thin strip from the back faces of the leaves. Although it is easy to verify this property for the simple shape class of extrusions, it is not obvious for arbitrary genus-0 orthogonal polyhedra, but was proven true in [DFO07].

2.1.3 Internal Node Unfolding

Having established a spiral path for each leaf node, we then extend these paths to the *internal* nodes in T, where an internal node is any non-leaf node other than the root. We process internal nodes of T in order of increasing height of their corresponding subtrees. This guarantees that, at the time an internal node b is processed, its children in T have already been processed. We assume inductively that having processed a front (back) child of b, the two endpoints of each spiral path originating at a leaf in the child's subtree are located side-by-side on the front (back) rim of b. The goal in processing b is to extend these paths so that the pairs of endpoints lie side-by-side on the top of b's rim segment shared with b's parent. In Figure 2 for example, b_1'' would have already been processed at the time b_1' is processed, and the paths need to be extended across b_1' to the front rim of b_1' shared with its parent b_9. The total number of spiral paths handled at b is precisely the number of leaves in the subtree of T rooted at b.

Let r be the top rim edge shared by b with its parent in T. Refer to the band labeled b and the edge labeled r in Figure 4 (which shows the unfolding for the example from Figure 2). Let $\xi_1, \xi_2, \ldots,$ be the spiral paths corresponding to the back children of b, listed in the order in which they are encountered in a clockwise walk starting at the top left corner of b's back rim). Our construction of T guarantees that at least one such back spiral exists at each internal node in T.

For each $i = 1, 2, \ldots$, we extend both ends of ξ_i by tracing along both sides of an orthogonal path that makes one complete counterclockwise cycle around the

top, left, bottom and right faces of b, while displacing toward the front of b, until it reaches r. The complete cycle around b is important to ensure that the spiral can later be thickened to cover the entire surface of b (hence the need for at least one back child at each internal node). For $i > 1$, the orthogonal path corresponding to ξ_i runs alongside the orthogonal path corresponding to ξ_{i-1}, to ensure that the spiral paths do not cross one another. (In Figure 4, the spiral paths are labeled in several places, to permit easy tracing. Because ξ_i only moves parallel to the y axis and spirals counterclockwise around b, it can be laid flat in the plane as a staircase monotone in the x-direction.

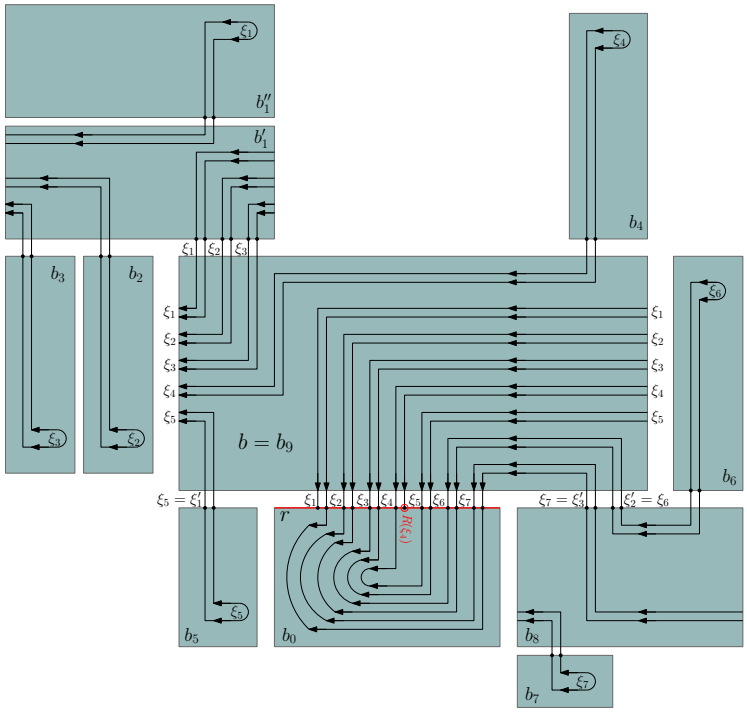

Fig. 4 Unfolding internal nodes and the root band (b_0) for the example from Figure 2; arrows indicate the direction followed by the unfolding algorithm.

We now turn to processing the spiral paths corresponding to the front children of b. Let $\xi_1', \xi_2', \ldots,$ be the front spiral paths encountered in this order in a counterclockwise walk around the front rim of b, starting at any point on the front rim of b. We extend both ends of each spiral ξ_i' by tracing along both sides of an orthogonal path that displaces slightly toward the back of b, then proceeds counterclockwise and toward the front of b until it meets r. Note that, if ξ_i lies to the left of r, then it will need to cycle around the top, left, bottom and right faces of b, in order to meet r (see spiral $\xi_1' = \xi_5$ in Figure 4). Again, care must be taken to ensure that the orthogonal path corresponding to ξ_i' does not cross any of the orthogonal paths corresponding to the other (front and back) spiral paths.

2.1.4 Root Node Unfolding

The last internal node of T whose spiral paths are extended to its parent in this fashion is the (single) child b of the root band. As described, these spiral paths cycle counterclockwise on b to reach the top rim segment r on the front rim of b, which by definition is the back rim of the root band. Let $\xi_1, \xi_2, \ldots, \xi_\ell$ be the extended spiral paths listed in the order encountered in a clockwise walk around the front rim of b, starting at the top left corner of the root's back face. Here ℓ is the number of leaf nodes in T. (For example, $\ell = 7$ in the example from Figure 4.) Let $L(\xi_i)$ be the left endpoint of spiral ξ_i on r and let $R(\xi_i)$ be the right endpoint. With this notation, the endpoints from left to right on r are $L(\xi_1), R(\xi_1), L(\xi_2), R(\xi_2), \ldots, L(\xi_\ell), R(\xi_\ell)$.

The next step of the algorithm is to link these ℓ spiral paths into a single path ξ that can be flattened in the plane as a monotone staircase. The starting point of ξ is $L(\xi_1)$, and the first part of ξ consists of ξ_1 followed by ξ_ℓ. These two spiral paths are linked via a connector path on the root band that extends from endpoint $R(\xi_1)$ to endpoint $R(\xi_\ell)$. See the 2D representation of the connector path linking the right endpoint of ξ_1 to the right endpoint of ξ_7 in Figure 4. This connector path is analogous to the connector paths followed at the leaf nodes, but here the vertical segment is on the front face of the root band. Because the root node has degree one and its only child is adjacent on its back rim, the root's front rim encloses a face of P, and so it is possible for the path to connect in this manner. This connector path is depicted in Figure 5. From $R(\xi_\ell)$, the connector path cycles counterclockwise to reach $R(\xi_1)$. From there, both parts of the path (i.e., the extensions of $R(\xi_\ell)$ and $R(\xi_1)$) cycle counterclockwise together towards the front face. The part of the path extending from $R(\xi_\ell)$ meets the front face vertical segment at its top endpoint, while the other part of the path extending from $R(\xi_1)$ continues cycling to the bottom face and meets the vertical segment at its bottom endpoint. (Observe that this path is a mirror image of the one depicted in Figure 3.) Like a leaf node connector path, this path can be laid flat in the

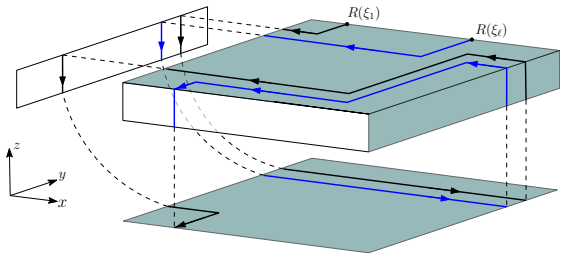

Fig. 5 The connector path for the spiral paths ξ_1 and ξ_ℓ; arrows indicate the direction followed by the unfolding algorithm, up to the vertical segment on the front face.

plane as a monotone staircase. Because the counterclockwise cycling direction of the connector path is consistent with that of ξ_1 and ξ_ℓ, ξ_1 can be laid flat on one side of the path and ξ_ℓ can be laid flat on the other side, thus forming a single monotone staircase. In this way we link ξ_1 and ξ_ℓ to form the first part of ξ.

Continuing to link the spiral paths to form ξ, $L(\xi_\ell)$ is linked to endpoint $L(\xi_2)$ using a connector path that runs alongside the previous connector path. Similarly,

this connector path flattens to a monotone staircase and connects the two flattened staircases ξ_ℓ and ξ_2. The remaining endpoints are paired up similarly and linked with connector paths. Specifically, $R(\xi_i)$ is linked to $R(\xi_{\ell-i+1})$ and $L(\xi_i)$ is linked to $L(\xi_{\ell-i+2})$), for $i = 2, 3, \ldots$ until one unpaired endpoint remains: $L(\xi_{\ell/2+1})$ (if ℓ is even) or $R(\xi_{(\ell+1)/2})$ (if ℓ is odd). This endpoint is where ξ terminates. See $R(\xi_4)$ in Figure 4.

2.1.5 Completing the Unfolding

To complete the unfolding of P, the spiral ξ is thickened in the $+y$ and $-y$ direction so that it completely covers each band. This results in a thicker strip, which can be unfolded as a staircase in the plane. Then the forward and rearward faces of P are partitioned by imagining the band's top rim edges illuminating downward light rays in these faces. The illuminated pieces are then "hung" above and below the thickened staircase, along the corresponding illuminating rim segments that lie along the horizontal edges of the staircase.

2.2 Unfolding Genus-0 Orthogonal Polyhedra

The unfolding algorithm described in subsection 2.1 for extrusions generalizes to all genus-0 orthogonal polyhedra as described in [CY15], so we briefly present the main ideas here and refer the reader to [CY15] for details.

Instead of partitioning P into boxes, the unfolding algorithm partitions P into slabs as defined in Section 1. It then creates an unfolding tree T in which each node corresponds to either an outer band (surrounding a slab) or an inner band (surrounding a hole). Each edge in T corresponds to a z-beam, which is a thin vertical rectangular strip from a frontward or rearward face of P connecting a parent's rim to a child's rim. Note that a z-beam may have zero geometric height, when two rims share a common segment. The spiral paths connect vertically along the z-beams when transitioning from a child band to its parent. For a parent band b, its front (back) children are those whose z-beams connect to b's front (back) rim. It was established in [DFO07] that the back rim of each leaf node in T encloses a face of P.

2.2.1 Assigning Unfolding Directions

Unlike the case of extrusions, where all bands are unfolded in the same direction (i.e., either all counterclockwise or all clockwise), general genus-0 orthogonal polyhedra may require different unfolding directions for different bands. For example, if a z-beam is incident to a top rim edge of the parent and a bottom rim edge of the child, then the unfolding direction (viewed from $y = -\infty$) changes when transitioning from the child to the parent. Figure 6 shows such an example: the z_1-beam is incident to a top rim edge of parent b_0 and a bottom rim edge of child b_1 (see the unfolding tree in Figure 6b, which shows the parent-child relationship); the unfolding direction is counterclockwise on b_1 and clockwise on b_0.

We assign unfolding directions for each band in a preorder traversal of the unfolding tree T. Set the unfolding direction for the root band to counterclockwise. At each band node b visited in a preorder traversal of T, if the edge in T connecting

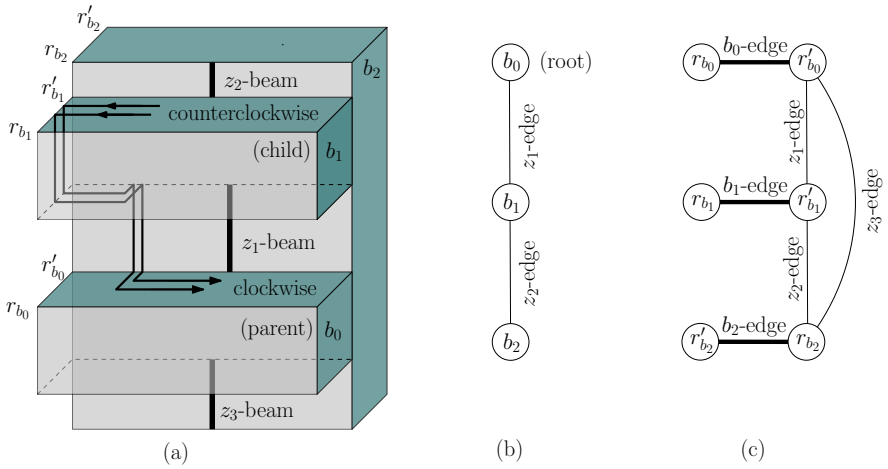

Fig. 6 (a) The unfolding direction changes when transitioning from child b_1 to parent b_0, the root node in this example; bands, rims and z-beams have been assigned indices consistent to those in (b) and (c) of this figure (b) Unfolding tree T (c) rim graph G_r, with b-edges marked thick and z-edges thin.

b to its parent corresponds to a z-beam incident to both top and bottom rim points, then set the unfolding direction for b to be opposite to the one for the parent (i.e., if the unfolding direction for the parent is counterclockwise, then the unfolding direction for b will be clockwise, and vice versa.) Otherwise, the endpoints of the z-beam connecting b to its parent are both top rim points or both bottom rim points, and in that case b inherits the unfolding direction of its parent. (Recall that a z-beam can have zero geometric height where two rims overlap.)

2.2.2 The Unfolding Procedure

The unfolding of a leaf band b follows the description in subsubsection 2.1.2 (Figure 4), except that the unfolding proceeds in the direction d assigned to b (as described in subsubsection 2.2.1), and the spiral path may cycle around multiple band faces instead of just four. When the two endpoints reach the z-beam on b's front rim, they track vertically along the z-beam, stopping side-by-side on the rim of b's parent.

At each internal node b in T, the unfolding proceeds as described in subsubsection 2.1.3. Observe that there is a natural cyclic ordering of b's front (back) children that is determined by their z-beam connections around b's front (back) rim, which guides the order in which we process b's children. Once the pairs of endpoints reach the z-beam connection to b's parent on b's front rim, they move vertically along the z-beam, stopping on the rim of b's parent. At the root node, these strips are glued together as described in subsubsection 2.1.4 (with the notion of "left" and "right" altered to match the cyclic ordering of the children, so that $L(\xi)$ and $R(\xi)$ are always encountered in this order in a clockwise walk along the rim). In addition, the spiral paths followed on inner bands are the same as those described previously for outer bands. For example, assume that the inner band b_{22} that forms a dent in the example from Figure 1 is a leaf band in T. Note that the

interior of P surrounds b_{22} on all sides, except for the front which is the entrance to the dent. Then the connector path is the same as in Figure 3a but is now viewed as cycling on the surface of P inside the dent.

In the unfolded staircase, the portion of ξ on a z-beam corresponds to a vertical riser. Thickening ξ proceeds as in the case of extrusions. The partitioning of the forward and rearward faces also follows the case of extrusions, but in addition to shooting illuminating rays down from top rim edges, bottom rim edges also shoot rays downward to illuminate portions of faces not illuminated by the top edges. The face pieces resulting from this partitioning method are hung above and below the staircase, as in the case of extrusions, as described in [DFO07].

3 Unfolding Genus-2 Orthogonal Polyhedra

The unfolding algorithm described in Section 2 depends on two key properties of P that are not necessarily true if P has genus 1 or 2. First, it requires the existence of a band with a rim enclosing a face of P that can serve as the root node of T. And second, it requires the back rim of each leaf node in T to enclose a face of P. These two requirements are needed so that the connector paths can use vertical strips on the enclosed faces in the unfolding. As a simple example of a genus-1 polyhedron for which neither property holds, consider the case when P is a box with a y-parallel hole through its middle. Slicing P with y-perpendicular planes results in a single slab having one outer and one inner band. In this case, no rim encloses a face of P. If we rotate P so that the hole is parallel to the x axis instead, slicing produces four bands, and the band surrounding the frontward (or rearward) box could serve as the root node. But every unfolding tree for the four bands contains a leaf whose back rim doesn't enclose a face of P.

In this section, we first show that there always exists an orientation for P such that at least one band has a rim enclosing a face of P that can be used for the root of T. Then we describe an algorithm that computes an unfolding tree for which we can prove that the number of leaf bands whose back rims do not enclose a face of P is at most g, where g is the genus of P. Finally, we describe changes to the unfolding algorithm that allow it to handle up to g leaves that don't enclose a face of P, for $g \leq 2$.

3.1 The Rim Unfolding Tree T_r

In order to establish these new results, we need finer-grained structures than the band-based G and T, which we call G_r and T_r, both of which are rim-based. We define the *rim graph* G_r for P in the following way. For each band b of P, add two nodes r_b and r'_b to G_r corresponding to each of b's rims. Add an edge connecting r_b and r'_b and call it a *band edge*, or a *b-edge* for short. For each pair of rims that can be connected by a z-beam, add an edge between them in G_r, and call it a *z-beam edge*, or a *z-edge* for short. Figure 6 illustrates these definitions; for more complex examples, see Figures 10 and 12. When referring to G_r, we will use the terms node and rim interchangably. For any simple *cycle* C in G_r, we distinguish between b-nodes of C, which are endpoints of b-edges in C, and z-nodes of C,

incident to two adjacent z-edges in C. For any subgraph $J \subseteq G_r$, we use $V(J)$ and $E(J)$ to denote the set of nodes and the set of edges in J, respectively.

Call a rim of G_r that encloses a face of P a *face-node*. A *nonface-node* in G_r is a node whose rim does not enclose a face of P. In Figure 6 for instance, r_{b_0}, r_{b_1} and r'_{b_2} are face-nodes, and r'_{b_0}, r'_{b_1} and r_{b_2} are nonface-nodes.

Proposition 1 *A rim r is a face-node of G_r if and only if every z-beam extending from a horizontal edge of r and going up or down on the surface of P hits r. A face-node of G_r is necessarily of degree one.*

Lemma 1 *If polyhedron P has genus $g \leq 2$, then there is a direction for slicing P such that G_r includes a face-node r_F.*

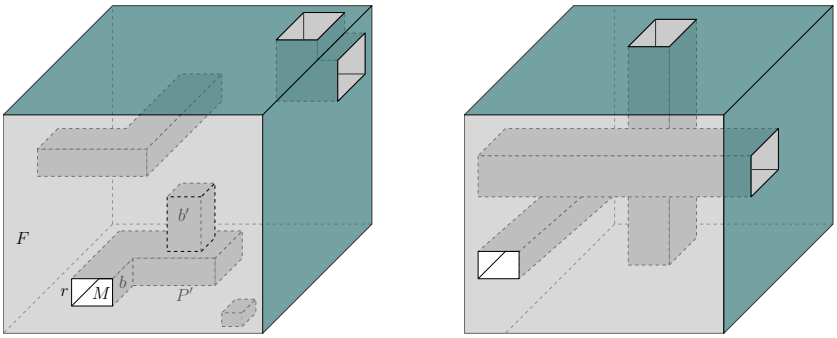

(a) (b)

Fig. 7 (a) A genus-2 polyhedron P with six extreme faces, all non-simply connected, that includes a genus-0 cave P' with mouth M (b) Lemma 1: a polyhedron of genus $g = 3$ with no slicing direction that yields a face-node.

Proof Define the *extreme faces* of P as those faces flush with the smallest bounding box enclosing P. There must be at least one extreme face in each of the six directions $d \in \{\pm x, \pm y, \pm z\}$. If any extreme face F, say in direction d, is simply connected, then slicing P with a d-plane (parallel to F) just adjacent to F will create a band b one of whose rims r_F encloses F. Thus, slicing P with d-planes will result in G_r including the face-node r_F, and the lemma is established.

Assume henceforth that each of the at least six extreme faces of P is not simply connected. So each extreme face F includes at least one inner band b. We now classify these bands b into two types.

Let r be the rim of an inner band b in face F. If cutting along r separates the surface of P into two pieces, P' which includes b, and the remainder $P \setminus P'$, then we say that b is a *cave-band*. Let M be the "mouth" of the cave: the portion of the Y-plane enclosed by the rim r. P' is a "cave" in the sense that an exterior path that enters through M can only exit P' back through M again. See Figure 7a. A band b that is not a cave-band is a *hole-band*. These have the property that there is an exterior topological circle that passes through the mouth M once, and so exits P' elsewhere.

Let P' be a cave with mouth M. $P' \cup M$ is an orthogonal polyhedron P'_M, inverting what was exterior to P to become interior to P'_M. Say that cave P' has genus 0 if P'_M has genus 0. We now claim that the lemma is satisfied if P has a genus-0 cave. For we may apply the same procedure to P'_M: Examine its extreme faces (one of which is M). If any extreme face (other than M) is simply connected, we are finished. Otherwise, each extreme face includes an inner band b'. It cannot be the case that b' is a hole band, for then P'_M has genus greater than 0. Moreover, b' cannot be a cave band for a cave of genus greater than 0. For in both cases, we could cut a cycle on the surface of P' that would not disconnect P'. So b' must determine a genus-0 cave band, and the argument repeats. Eventually we reach a simply connected extreme face.

Now we have reduced to the situation that each of P's six or more extreme faces contains either a hole-band, or a genus-(≥ 1) cave band. Let the number of these bands be h and c respectively. We now account for the genus g of P, and the number of extreme faces. Each cave of genus-(≥ 1) contributes at least 1 to g. A hole-band in an extreme face could exit through that same face, or exit through a different extreme face, or exit through a non-extreme face. In the first two cases, two hole-bands contribute 1 to g; in the third case, one hole band contributes 1 to g. So h hole-bands contribute at least $h/2$ to the genus, and we have the inequality $c + h/2 \leq g \leq 2$.

We have defined h and c to be the number of such bands in extreme faces, and we know that each of the at least six extreme faces must have one or more hole- or genus-(≥ 1) cave-bands. So we must have $c + h \geq 6$. But these two inequalities have no solutions in non-negative integers. □

Figure 7b shows that Lemma 1 is tight. Henceforth we assume P is oriented so that the direction guaranteed by the lemma slices P with Y-planes, and so G_r has a face-node r_F. This node will become the root of the unfolding tree.
Figure 8 shows an example of a genus-2 polyhedron sliced with Y-parallel planes in the direction identified by Lemma 1, which yields two face-nodes r_1 and r'_7. The rim graph G_r for this polyhedron is depicted (ahead) in Figure 12b, with r_1 selected as root.

Lemma 2 *G_r is connected and contains no nonface-leaf nodes.*

Proof Call a maximal connected surface piece of P located in a plane Y_i a *z-patch* (suggestive of the fact that it might contain z-beams). First note that the subset of rims belonging to a z-patch induces a connected component in G_r (call it a *z-patch component*) that contains z-edges only. For example, the front face of band b_5 in Figure 10 is a z-patch that connects rims r'_1 and r'_4 to r_5 with z-beams.

The connectedness of P's surface implies that all z-patches are connected together by bands. In G_r, this corresponds to all z-patch components being connected together by b-edges. It follows that G_r is connected.

Next we show that there are no nonface-leaves in G_r. Suppose there is a node r in G_r of degree 1 that does not enclose a face of P. Because all nodes in G_r are connected by a b-edge to the rim on the other side of the band, there is a b-edge adjacent to r. Now consider extending z-beams up and down from every horizontal edge of r. Because r does not enclose a face of P, at least one of the z-beams must hit the rim of another band by Proposition 1. But then r also has a z-edge adjacent to it, giving it a degree of at least 2, a contradiction. □

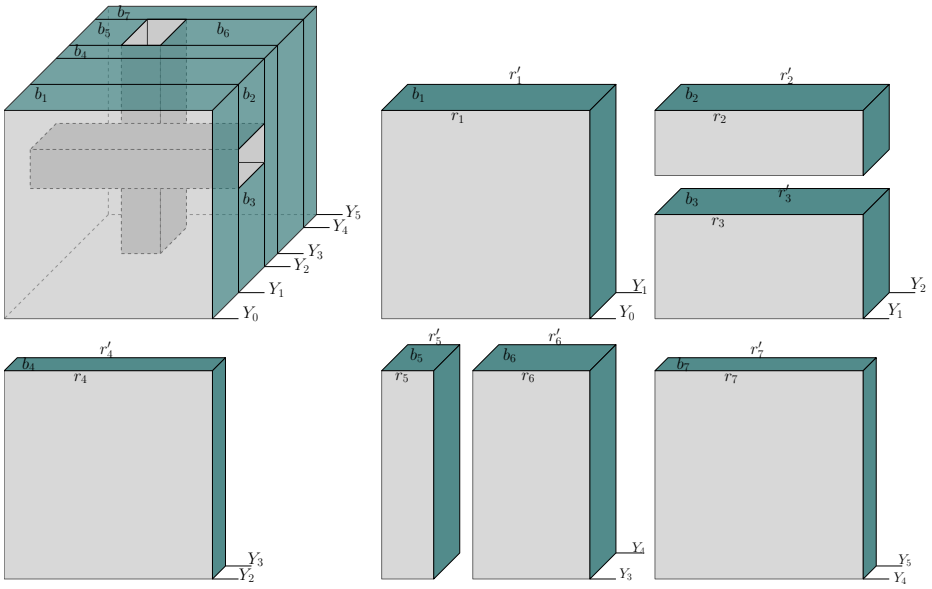

Fig. 8 Genus-2 polyhedron partitioned into slabs.

Note that G_r for the genus-3 example in Figure 7b has no leaf nodes at all, and so satisfies this lemma vacuously.

Our next goal is to find a rim spanning tree T_r of G_r with at most g nonface-leaves, which will ultimately similarly limit the number of nonface-leaf nodes of T. The RimUnfoldingTree method for achieving such a T_r is outlined in Algorithm 1. It reduces G_r to a tree by repeatedly removing a z-edge from an existing cycle, thus breaking the cycle. In addition, it does this in such a way that at most g nonface-leaf nodes are created. If we were to break a cycle by removing an arbitrary z-edge from it, it may be that both endpoints of the z-edge have degree two, and thus removing it would result in the creation of two new leaf nodes, both of which would be nonface-nodes. To avoid this, our RimUnfoldingTree algorithm strategically selects a z-edge e with at least one endpoint, say u, of degree 3 or more. Thus the removal of e results in the creation of at most one new leaf. More importantly, the algorithm ensures that one of u's three or more adjacent edges is an edge that is not part of any current (simple) cycle. Call this edge e', and note that e' will never be removed by the algorithm, because the algorithm only removes cycle edges. The existence of e' guarantees that u's degree will not drop below 2 (for if the degree of u were to reach 2, then because one of the two adjacent edges is e' and not part of a cycle, the other adjacent edge cannot be part of a cycle either, and therefore neither edge will be removed). This property of u will be important in bounding the number of nonface-leaf nodes created by the algorithm.

Let us walk through a few iterations of the RimUnfoldingTree algorithm with the help of the example from Figure 9. The initial graph $T_r = G_r$ and the subgraph (not necessarily connected) induced by its cycles are shown in Figure 9a. The nodes r'_1, r_4, r'_4, and r_7 in H are all candidates for the selection of u in the first iteration of the algorithm, and the algorithm picks one of them – say, $u = r'_1$

T_r = RimUnfoldingTree(G_r)

Initialize $T_r \leftarrow G_r$
while T_r *is not a tree* **do**
  Let $H \subset T_r$ be the subgraph of T_r induced by all simple cycles in T_r
  Pick an arbitrary node $u \in V(H)$ incident to an edge e' in $E(T_r) \setminus E(H)$
  Pick an arbitrary z-edge $e \in E(H)$ incident to u
  Remove e from T_r
end
return T_r

Algorithm 1: Computing a rim spanning tree of G_r.

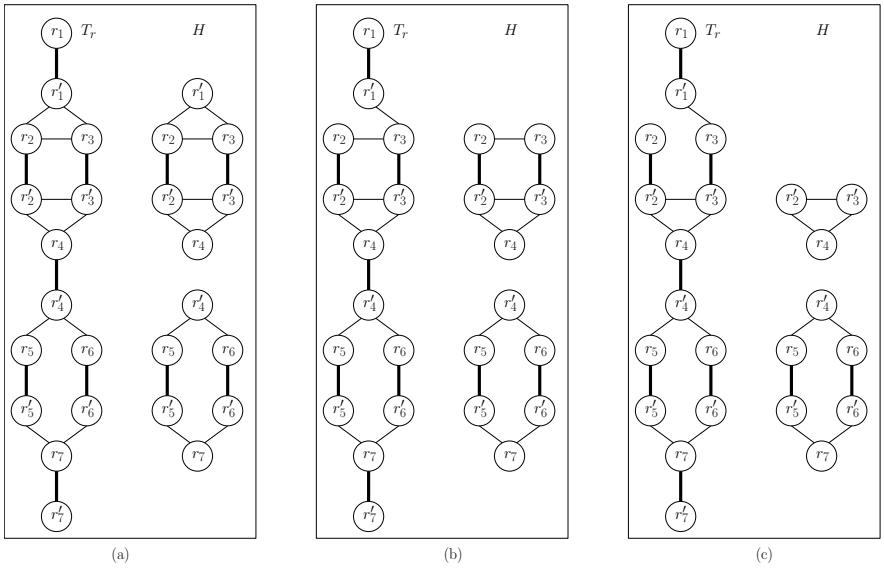

Fig. 9 Algorithm RimUnfoldingTree (a) T_r and H at the beginning of the first iteration: the algorithm identifies $e = (r'_1, r_2)$ to be removed from T_r (b) T_r and H at the beginning of the second iteration: the algorithm identifies $e = (r_3, r_2)$ to be removed (c) T_r and H at the beginning of the third iteration: the algorithm identifies $e = (r'_3, r_4)$ to be removed, and so on.

– arbitrarily. This node is incident to two z-edges (r'_1, r_2) and (r'_1, r_3) of H, so the algorithm picks one of them – say, (r'_1, r_2) – arbitrarily, and removes it from T_r. The resulting T_r, and the subgraph induced by its cycles, are shown in Figure 9b. At this point, nodes r_3, r_4, r'_4, and r_7 are candidates for the selection of u in the second iteration of the algorithm, and the algorithm picks one of them – say, r_3 – arbitrarily. This node is incident to a single z-edge (r_3, r_2) of H, so the algorithm removes it from T_r. The resulting T_r, and the subgraph induced by its cycles, are shown in Figure 9c. This process continues in a similar way, until T_r contains no cycles. A valid output produced by this algorithm is shown in Figure 12c.

Lemma 3 *The* RimUnfoldingTree *algorithm produces a spanning tree of* G_r.

Proof By Lemma 1, G_r (and therefore T_r) includes a node of degree one that is not part of a cycle in G_r and therefore is not in H. This implies that there is at least one edge in $E(T_r) \setminus E(H)$ incident to a node u of H (because T_r is

connected). This proves the existence of the node u picked in each iteration of the RimUnfoldingTree algorithm. Because u is part of at least one cycle in H, its degree is at least two in H. The edge in $E(T_r) \setminus E(H)$ incident to u contributes another unit to the degree of u; therefore u has degree at least three in T_r. By the definition of G_r, no two b-edges in G_r are adjacent, since any two b-edges are connected by a path of one or more z-edges in G_r. (Recall a z-edge might have zero geometric height, when two rims share a common segment.) This implies that, out of the two or more edges in $E(H)$ incident to u, at least one is a z-edge. This proves the existence of the edge e picked in each iteration of the RimUnfoldingTree algorithm. Removing e from T_r breaks at least one cycle in H, so the size of H decreases in each loop iteration. It follows that the RimUnfoldingTree algorithm terminates and produces a tree T_r that spans all nodes of G_r. □

Theorem 1 *The number of nonface-leaves in the rim tree T_r produced by the* RimUnfoldingTree *algorithm is no greater than the genus g of P.*

Proof Consider a z-edge $e = (u, v)$ removed from T_r in one iteration of the RimUnfoldingTree algorithm. The node u is incident to at least two edges in $E(H)$ and at least one edge in $E(T_r) \setminus E(H)$; therefore its degree is at least three in T_r. The removal of e from T_r leaves u of degree at least two, so u does not become a leaf in T_r. This argument holds even if u is picked repeatedly in future iterations of the RimUnfoldingTree algorithm, so u will not become a leaf in T_r.

If v has degree three or more in T_r prior to removing e from T_r, then v does not become a leaf after removing e. So suppose that v has degree two in T_r before removing e. Recall that every node in G_r is connected by a b-edge to the other rim of its band. Because the RimUnfoldingTree algorithm never removes a b-edge, this property holds in T_r as well. It follows that the other edge incident to v (in addition to the z-edge e) must be a b-edge. Hence any leaf node in T_r created by the RimUnfoldingTree algorithm is an endpoint of a b-edge in T_r.

By Lemma 2, G_r does not include any nonface-leaves, so any nonface-leaves in T_r must have been created by the RimUnfoldingTree algorithm. Let $r_1, r_2, \ldots, r_k$ be the set of leaves in T_r created by the RimUnfoldingTree algorithm. If $k \leq g$, then the theorem is true.

Assume now that $k > g$. For each i, let b_i be the band with rim r_i. Because T_r includes all the b-edges from G_r, it must be that T_r includes the b-edge (r_i, r_i') corresponding to b_i, so the parent r_i' of r_i in T_r is the other rim of b_i. For each $i = 1, 2, \ldots, k$, we perform a cut on P's surface along a closed curve around the middle of b_i, between its rims r_i and r_i'. Refer to Figure 10a, which shows the cuts around the middle of b_1 and b_2 as dashed lines. Note that r_1 and r_2 are nonface-nodes corresponding to b_1 and b_2 respectively, as inferred from the rim unfolding tree T_r shown in Figure 10b (edges of T_r are marked solid, with b-edges thicker than z-edges). We now show that these cuts do not disconnect the surface of P, contradicting our assumption that $k > g$.

To see this, consider any two points c_i and c_i' on b_i that are separated by the cut around b_i, with c_i on the same side of the cut as r_i, and c_i' on the same side of the cut as r_i'. Let $e_i = (r_i, u_i)$ be the z-edge whose removal from T_r created the leaf r_i (so u_i here plays the role of u in the RimUnfoldingTree algorithm, and by our observation above, u_i is not a leaf in T_r). We construct a path p_i on the surface of P connecting c_i to c_i' as follows: the path p_i starts at c_i, moves towards r_i and along the z-beam corresponding to e_i to the rim u_i, then follows the path

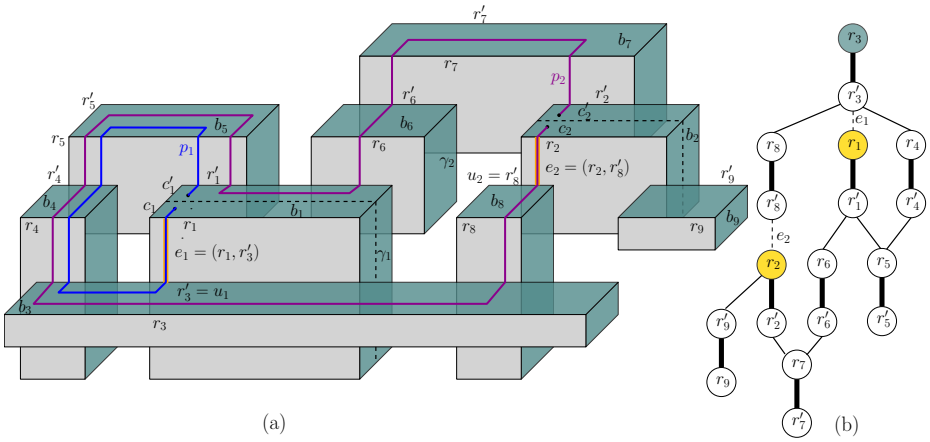

Fig. 10 Theorem 1 (a) example polyhedron of genus 2; cuts around the middle of bands b_1 and b_2 are marked with dashed lines (b) Rim tree T_r with root r_3 and 2 nonface-leaves, r_1 and r_2. Thick and thin edges are band- and z-edges respectively.

in T_r from u_i to the rim r'_i, and finally across b_i to c'_i. See Figure 10, which traces the paths p_1 and p_2 on the polyhedron surface. Note that r_i is the only leaf visited by p_i (because u_i is not a leaf), so p_i does not cut across any of the leaves r_j, for $j \neq i$. This implies that p_i connects c_i and c'_i in the presence of all the other cuts. Since this is true for each i, we conclude that these cuts leave the surface of P connected, contradicting our assumption that $k > g$. □

3.2 The Unfolding Algorithm

Let T_r be the rim tree computed by the RimUnfoldingTree algorithm described in subsection 3.1. We pick the root of T_r to be a face-node identified by Lemma 1, and call its corresponding band the *root band*. This guarantees that the front face of the root band is a face of P and thus it can be used in constructing the connector paths linking the spiral paths associated with the root's children.

For ease in describing the modified spiral paths we use for genus-1 and genus-2 polyhedra, we first convert T_r into a standard unfolding tree T having bands for nodes rather than rims. We do this by simply contracting the b-edges. Specifically, we replace each b-edge (r_i, r'_i) and its two incident nodes r_i and r'_i by a single node b_i whose incident edges are the z-edges incident to r_i or r'_i. Let T be the tree resulting from T_r after contracting all the b-edges, with its root node corresponding to the root band. For example, Figure 12d (ahead) shows the tree T obtained by contracting b-edges of the tree T_r in Figure 12c. The two pairs of boxed nodes will be explained shortly.

Observe that the edges in T are in a one-to-one correspondence with the z-edges in T_r. For example, consider a z-edge (r_i, r_j) in T_r such that node r_i is the parent of r_j. Then in T, there is an edge (b_i, b_j) where b_i is the parent of b_j. Furthermore, r_j is the front rim of b_j because of the z-beam connection to its parent determined by the z-edge (r_i, r_j). Any other nodes adjacent to b_j in T are its front or back children, depending on whether the corresponding z-edges in T_r

connect to its front rim (r_j) or its back rim. In this way, the rim connections that are explicitly represented in T_r are preserved in T through the assignment of front and back rims/children.

There is not, however, an immediate one-to-one correspondence between leaf nodes in T_r and leaf nodes in T. If r'_i is a leaf in T_r and its parent r_i has no other children, then clearly b_i in T has degree 1, and we note that its back rim is r'_i. See, for example, the leaf r_5 in Figure 12c (ahead) and the corresponding leaf b_5 in Figure 12d. But suppose r_i has one or more other children in T_r besides the leaf r'_i. Then these other children are connected via z-edges to r_i, and node b_i in T has degree greater than 1 and is not a leaf. Specifically, b_i in T has one or more front children connected via z-beams to its front rim r_i, and it has no back children (because its back rim r'_i is a leaf in T_r). This is the case for the leaf node r_2 from Figure 12c, whose parent node r'_2 has another child r_4; the corresponding node b_2 in T is not a leaf in T. Similarly, the parent r_7 of leaf node r'_7 from Figure 12c has another child r'_5, and the corresponding node b_7 is not a leaf in T. But we handle this in the same way as in a standard unfolding tree (as described in subsubsection 2.1.1) by splitting band b_i into two bands b'_i and b''_i. In T, b_i is replaced by b'_i and has b''_i as a back leaf child. See Figure 12d, which shows node b_2 split into b'_2 and b''_2, and node b_7 split into b'_7 and b''_7. The front rim of b'_i is rim r_i and the back rim of b''_i is rim r'_i. In this way, each leaf r'_i in T_r has a corresponding leaf node in T whose back rim is r'_i, and vice versa. If r'_i is a nonface-leaf in T_r, then we will also say the corresponding leaf in T is a nonface-leaf, meaning that its band's back rim does not enclose a face of P. These observations, along with Theorem 1, establish the following corollary.

Corollary 1 *The number of nonface-leaves in the unfolding tree T is at most g, where $g \geq 0$ is the genus of P.*

Using T, we assign unfolding directions to each band as described in subsubsection 2.2.1. If T has no nonface-leaves, then we complete the unfolding of P using the linear unfolding algorithm from [CY15] (as summarized in Section 2). We now show how to modify the unfolding algorithm to handle the cases when T has one or two nonface-leaves. Because a nonface-leaf b has a back rim that does not enclose a face of P, there might be no vertical back face segment available for b's connector path. For these leaves, we use a spiral path that has one endpoint on b's back rim and the other endpoint on b's front rim. The path cycles around the band faces in the unfolding direction of b from the back point to the front point. (In Figure 3, this would be just the portion of the path that extends from the top of the back rim to endpoint e_1.) Corollary 1 implies that this can occur for at most two leaves in T (since we assume P to have genus $g \leq 2$). For all face-leaves, we proceed as before in extending both ends of the spiral path from the band's back rim to its front rim. Figure 12a shows examples of the spiral paths for nonface-leaves b_5 and b''_2 and face-leaf b''_7. For b_5 (b''_2), the end of its path located on its back rim is labeled t_2 (t_1); from t_2 (t_1) the path is shown cycling clockwise to the front rim. For b''_7, it uses a connector path which allows both ends to cycle to its front rim, as illustrated on its top and bottom faces.

The processing of internal nodes is handled as before by extending the spiral paths towards the root. The only difference is that for the (at most 2) spiral paths originating at nonface-leaves, there is only one end of the path to extend. After processing the internal nodes, the ends of the spiral paths are at the root band.

Specifically, each spiral path originating at a face-leaf has two endpoints located on the back rim of the root band, and each spiral path originating at a nonface-leaf has one endpoint located on the back rim of the root band. The challenge here is to connect all these spiral paths together at the root band into a single final strip that starts on the back rim of one nonface-leaf and (if there is a second nonface-leaf) ends on the back rim of the other. (This is one place where the assumption that $g \leq 2$, and so there are at most two nonface-leaves (by Corollary 1), is crucial.) Because the front rim of the root node does enclose a face of P, it is possible to use strips from its enclosed face for the connectors.

3.2.1 Root Node Unfolding: One Nonface-Leaf Case

First we describe how to link the leaves' extended spiral paths together at the root node, and unfold the root band in the process, for the case when T has exactly one nonface-leaf. Let $\xi_1, \xi_2, ..., \xi_\ell$ be the spiral paths corresponding to the ℓ face-leaves in T (excluding the one nonface-leaf). After processing all the internal nodes, the two ends of each of these spiral paths are located side-by-side on the back rim r of the root band, as previously illustrated in Figure 4. Let t be the spiral path corresponding to the nonface-leaf. One end of t is on r, and the other end is on the back rim of its leaf. If $\ell > 1$, we assume the spiral paths of the face-leaves are labeled in clockwise order around the root's back rim, with t located in the middle between $\xi_{\lceil \ell/2 \rceil}$ and $\xi_{\lceil \ell/2 \rceil + 1}$. We then begin by linking all these spiral paths into one strip ξ as described in subsubsection 2.1.4 for the case when there are no nonface-leaves. I.e., starting with the pair $R(\xi_1)$ and $R(\xi_\ell)$, the ends of the spiral paths are paired up and linked together via connector paths. (Recall that, for each ξ_i, the endpoints $L(\xi_i)$ and $R(\xi_i)$ are encountered in this order in a clockwise walk along the back rim of the root band, starting, say, at t or at a rim corner.) The only difference is that, with t in the middle between ξ_1 and ξ_ℓ, the last pair of spiral path endpoints linked together will be $R(\xi_{\lceil \ell/2 \rceil})$ and t when ℓ is odd, and t and $L(\xi_{\lceil \ell/2 \rceil + 1})$ when ℓ is even. The remainder of the unfolding is the same. Thus the resulting spiral ξ starts at $L(\xi_1)$ and ends on the back rim of the nonface-leaf.

3.2.2 Root Node Unfolding: Two Nonface-Leaves Case

We now discuss the more complex case when T has two nonface-leaves. In this case, the final spiral path will have its two ends on the back rims of the two nonface-leaves. Again let $\xi_1, \xi_2, ..., \xi_\ell$ be the spiral paths corresponding to the face-leaves, and let t_1 and t_2 be the spiral paths corresponding to the two nonface-leaves. We assume that t_1 and t_2 are labeled such that the number of spiral paths separating them counterclockwise from t_2 to t_1 on the root's back rim is at most $\lfloor \ell/2 \rfloor$. (If it is more than $\lfloor \ell/2 \rfloor$, then we just switch the labels of t_1 and t_2.) If $\ell > 1$, we further assume that the spiral paths of the face-leaves are labeled so that t_1 is in the middle between $\xi_{\lceil \ell/2 \rceil}$ and $\xi_{\lceil \ell/2 \rceil + 1}$. Observe that these labeling rules position t_2 on the portion of the rim counterclockwise between ξ_1 and t_1. See Figure 11 for an example with $\ell = 4$, which shows the root band, the spiral path endpoints t_1 and t_2 marked on the back rim of the root band, and the spiral paths $\xi_1, \ldots, \xi_4$ depicted as thick dotted arcs above the root band. Note that the counterclockwise ordering from ξ_1 along the rim is: $\xi_1, \ldots, t_2, \ldots, t_1$.

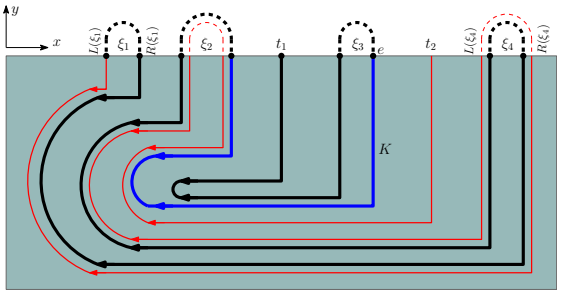

Fig. 11 Root band, with ξ consisting of the thick (black) and thin (red) paths. The thick (black) path connects $\xi_1, \ldots, \xi_4$ and t_1. The thin (red) path is the extension of ξ that connects $L(\xi_1)$ to t_2. For the two ends of each ξ_i, the dotted paths indicate the spiral path connecting them, which goes down to the associated leaf node and back.

We begin by linking the spiral paths $\xi_1, \ldots, \xi_\ell$ and t_1 into a single strip ξ as described in subsubsection 3.2.1 for the case of one nonface-leaf. (See the thick black/blue path marked on the root band in Figure 11, which shows the portion of ξ starting at $R(\xi_1)$ and connecting $\xi_1, \ldots, \xi_4$ and t_1.) Note that ξ has one end at $L(\xi_1)$ and the other end on the back rim of the nonface-leaf corresponding to t_1. Linking in t_2, however, requires some special handling. We will do this by extending ξ from its endpoint $L(\xi_1)$ all the way to t_2 by following alongside the portion of ξ that tracks from $R(\xi_1)$ to t_1, until t_2 is reached. (Refer to the thin red path in Figure 11.) At all times, this extension is tracing a new path on one side of the path it is following. Specifically, starting from $L(\xi_1)$, the extension first follows alongside the connector path linking $R(\xi_1)$ to $R(\xi_\ell)$. It then follows alongside the spiral path from $R(\xi_\ell)$ to $L(\xi_\ell)$, going all the way down to the leaf node corresponding to ξ_ℓ and then back up. It next follows alongside the connector path linking $L(\xi_\ell)$ to $L(\xi_2)$, and then alongside the spiral path from $L(\xi_2)$ to $R(\xi_2)$, and so on. This continues until the extension reaches the connector path, say K, that links to the end of the strip piece located immediately counterclockwise from t_2 on the rim. This connector is drawn blue in Figure 11. Because at most $\lfloor \ell/2 \rfloor$ spiral paths are located counterclockwise from t_2 to t_1, the strip piece located immediately counterclockwise of t_2 is either t_1 or one of $\{\xi_{\lceil \ell/2 \rceil + 1}, \xi_{\lceil \ell/2 \rceil + 2}, \ldots, \xi_\ell\}$. If it is one strip piece of the latter, say ξ_i, then the connector K links to $R(\xi_i)$. Let e be the end of the spiral path (t_1 or ξ_i) to which the connector K links.

When the extension reaches the connector path K, it follows alongside it, but instead of following it all the way to e, the extension continues past e until it reaches t_2, at which time it connects with t_2 and we are finished. This path is drawn with a thin red line in Figure 11: it starts at $L(\xi_1)$, follows alongside the thick black path that extends from $R(\xi_1)$ to $e = R(\xi_3)$, and from there it reaches t_2. The result is the final unfolding spiral ξ with one end on the back face of the nonface-leaf corresponding to t_1, and the other end on the back face of the nonface-leaf corresponding to t_2.

Figure 12 shows the complete spiral path for the genus-2 polyhedron from Figure 8, with the slabs slightly separated for clarity. In this example $\ell = 1$, ξ_1 corresponds to node b_7'' with back face-rim r_7', and the t_1 and t_2 paths correspond to b_2'' and b_5, with back nonface-rims r_2 and r_5, respectively. (For clarity, the paths

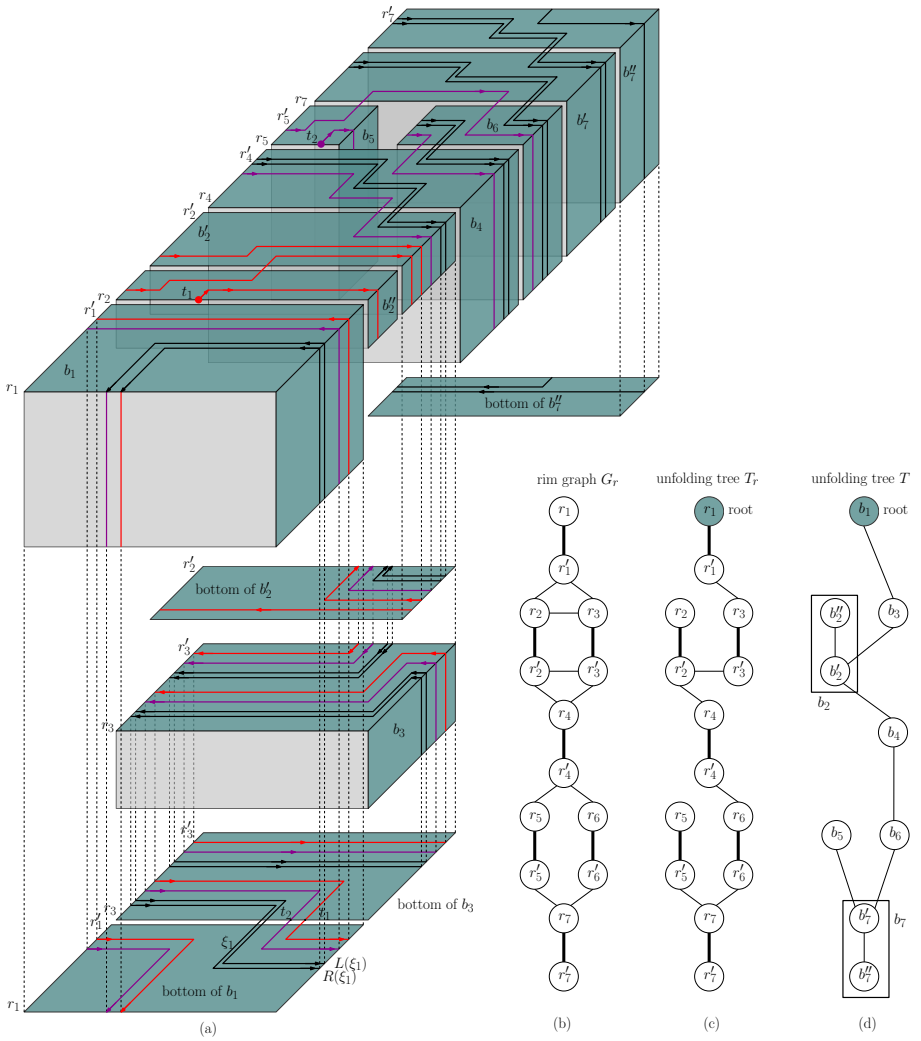

Fig. 12 Unfolding the genus-2 polyhedron from Figure 8, with slabs slightly separated for clarity (a) spiral path corresponding to the unfolding tree T from (d) of this figure; arrows indicate the direction followed by the unfolding algorithm; (b) rim graph G_r; (c) rim unfolding tree T_r (one of several possible) extracted from G_r by the RimUnfoldingTree algorithm; (d) unfolding tree T obtained by compressing b-edges of T_r and splitting internal nodes with no back children: b_1 is the root, b_2'' and b_5 are nonface-leaves, b_7'' is a face-leaf.

t_1 and t_2 are labeled on the bottom face of b_3, as they make the transition to the bottom face of b_1.)

3.3 Level of Refinement

Using the Chang-Yen algorithm [CY15], any genus-0 orthogonal polyhedron P can be unfolded using linear refinement. Specifically, they refine each rectangular face

of P via grid-unfolding using a $(2\ell \times 4\ell)$-grid, where ℓ is the number of leaves in T, and cuts are allowed along any of these grid lines. In the worst case, the algorithm presented here requires at most twice the level of refinement, i.e., $(4\ell \times 8\ell)$ refinement. This level of refinement is necessary when there are two nonface-leaves in T. In this case, the first part of the spiral path (from $L(\xi_1)$ to the end of t_1 located on the back rim of the first nonface-leaf is the same as in the Chang-Yen algorithm, but with care given to the order in which the spiral paths are connected and with only one endpoint of t_1 at the root. (This is the black and blue portions of the path illustrated in Figure 11.) Thus no additional refinement is necessary for this part of the path. The doubling of the refinement is due to the retracing of this path which is needed to extend it from $L(\xi_1)$ to t_2, the spiral path of the second nonface-leaf. (This is the red portion of the path in Figure 11.) Because the retracing follows alongside the existing path, it requires twice the refinement. Thus, the overall level of refinement is $(4\ell \times 8\ell)$, which is linear.

We conclude with this theorem:

Theorem 2 *Any n-vertex orthogonal polyhedron of genus $g \leq 2$ may be unfolded to a planar, simple orthogonal polygon of $O(n^3)$ edges, by cutting along a linear grid-refinement.*

The $O(n^3)$ bound follows from $O(\ell^2)$ grid edges per face, with $\ell = O(n)$ and $O(n)$ faces.

4 Conclusion

It is not evident how to push the techniques common to [DFO07], [DDF14], and [CY15] to unfold polyhedra of genus $g \geq 3$, the next frontier in this line of research. Both Lemma 1 (existence of a face-node to serve as root of T) and Theorem 1 (the RimUnfoldingTree algorithm leads to at most $g \leq 2$ nonface-leaves) are crucial in the unfolding algorithm described in Section 3. The final stitching together of the spiral paths relies on there being at most two nonface-leaves of the unfolding tree T.

On the other hand, it is not difficult to unfold the genus-3 polyhedron shown in Figure 7b in an ad-hoc manner. The challenge is to find a generic algorithm for genus-3 and beyond.

Acknowledgement. We thank all the participants of the 31st Bellairs Winter Workshop on Computational Geometry for a fruitful and collaborative environment. In particular, we thank Sebastian Morr for important discussions related to Theorem 1, and to the stitching of unfolding strips at the root node.

References

BDD+98. Therese Biedl, Erik Demaine, Martin Demaine, Anna Lubiw, Mark Overmars, Joseph O'Rourke, Steve Robbins, and Sue Whitesides. Unfolding some classes of orthogonal polyhedra. In *Proceedings of the 10th Canadian Conference on Computational Geometry*, Montréal, Canada, August 1998.

BDE+03. Marshall Bern, Erik D. Demaine, David Eppstein, Eric Kuo, Andrea Mantler, and Jack Snoeyink. Ununfoldable polyhedra with convex faces. *Computational Geometry: Theory and Applications*, 24(2):51–62, February 2003.

CY15. Yi-Jun Chang and Hsu-Chun Yen. Unfolding orthogonal polyhedra with linear refinement. In *Proceedings of the 26th International Symposium on Algorithms and Computation, ISAAC 2015, Nagoya, Japan*, pages 415–425. Springer Berlin Heidelberg, 2015.

DDF14. Mirela Damian, Erik D. Demaine, and Robin Flatland. Unfolding orthogonal polyhedra with quadratic refinement: the delta-unfolding algorithm. *Graphs and Combinatorics*, 30(1):125–140, 2014.

DFMO05. Mirela Damian, Robin Flatland, Henk Meijer, and Joseph O'Rourke. Unfolding well-separated orthotrees. In *Abstracts from the 15th Annual Fall Workshop on Computational Geometry*, Philadelphia, PA, November 2005.

DFO07. Mirela Damian, Robin Flatland, and Joseph O'Rourke. Epsilon-unfolding orthogonal polyhedra. *Graphs and Combinatorics*, 23(1):179–194, 2007.

DFO08. Mirela Damian, Robin Flatland, and Joseph O'Rourke. Unfolding Manhattan towers. *Computational Geometry: Theory and Applications*, 40:102–114, 2008.

DM04. Mirela Damian and Henk Meijer. Edge-unfolding orthostacks with orthogonally convex slabs. In *Abstracts from the 14th Annual Fall Workshop on Computational Geometry*, pages 20–21, Cambridge, MA, November 2004. `http://cgw2004.csail.mit.edu/talks/34.ps`.

DO07. Erik D. Demaine and Joseph O'Rourke. *Geometric Folding Algorithms: Linkages, Origami, Polyhedra*. Cambridge University Press, July 2007.

LPW14. Meng-Huan Liou, Sheung-Hung Poon, and Yu-Jie Wei. On edge-unfolding one-layer lattice polyhedra with cubic holes. In *The 20th International Computing and Combinatorics Conference (COCOON) 2014*, pages 251–262, 2014.